Coupled plasmon–LO-phonon modes at high-magnetic fields

A. Wysmołek,[1,2] D. Plantier,[1] M. Potemski,[1] T. Słupiński,[2] and Z. R. Żytkiewicz[3]
[1]*Grenoble High Magnetic Field Laboratory, MPI/FKF-CNRS, Boite Postale 166X, F-38042 Grenoble Cedex 9, France*
[2]*Institute of Experimental Physics, Warsaw University, Hoża 69, PL-00-681 Warszawa, Poland*
[3]*Institute of Physics, Polish Academy of Sciences, Aleja Lotnikow 32/46, 02-668 Warszawa, Poland*
(Received 2 June 2006; revised manuscript received 8 August 2006; published 20 October 2006)

High-magnetic-field (up to 28 T) inelastic light scattering experiments on coupled plasmon–LO-phonon modes in degenerate *n*-type GaAs are reported. The data are analyzed using a standard, dielectric function approach. Results obtained for samples with high electron concentration are well understood. A strong interaction of coupled LO-phonon-plasmon modes with the collective cyclotron resonance excitations (Bernstein modes) is observed. In samples with lower electron concentration, an unexpected Raman scattering signal in the vicinity of the undressed optical phonon is observed at high magnetic fields. A field induced metal-insulator transition is shown to be traced with Raman scattering experiments in samples with the lowest electron concentration.

DOI: 10.1103/PhysRevB.74.165206 PACS number(s): 78.30.Fs, 73.20.Mf, 78.20Ls

I. INTRODUCTION

Coupled plasmon–longitudinal optical (LO)-phonon modes are an interesting example of a classical problem in "wave propagation in solids."[1] These modes are intrinsic for metallic *and* polar semiconductors. The interaction between LO-phonons and plasmons occurs via "macroscopic" longitudinal electric fields produced by both excitations, resulting in new combined proper modes of the system.[2] These modes can be conveniently studied using the technique of inelastic light scattering as demonstrated in the pioneering work of Mooradian and Wright[3] and also shown in many other studies.[4–7]

The properties of a plasma subjected to a static magnetic field are significantly modified.[1,8] A magnetic field B applied to a metallic system introduces a characteristic frequency, namely the cyclotron frequency $\omega_c = eB/m^*$ of motion of the carriers (with an effective mass m^*) in the plane perpendicular to the field direction. In polar-semiconductor plasmas, by changing the magnetic field the cyclotron frequency ω_c can be made comparable to all important frequencies of the system, namely the plasma frequency ω_p, and the frequencies of longitudinal (LO) and transverse (TO) optical phonons. The physics of coupled plasmon phonon modes under these particular and interesting conditions has never been fully explored in Raman scattering experiments, although to a great extent considered in theory.[1,9]

In this paper we present systematic magneto-Raman scattering studies of coupled plasmon-phonon modes in bulk, *n*-type GaAs samples with different electron concentrations. Experiments were performed in a wide range of magnetic fields (up to 28 T) which cover the limit of cyclotron frequency exceeding the LO frequency of the insulating material. The data are analyzed using a classical approach of a dielectric function which is somewhat modified for the sake of our results, as compared to its original form developed for Maxwellian plasmas and in the limit of weak magnetic fields.[1] The results obtained on samples with high electron concentrations are well understood. Our notable observation is the effect of interaction between multiple collective cyclotron excitations (Bernstein modes[10]) and finite k-vector magnetoplasmon-phonon modes.[1] The interpretation of measured Raman spectra becomes less obvious for samples with progressively lower electron concentrations. The first complication encountered in samples which still remain metallic is the appearance, at high magnetic fields, of a Raman scattering signal in the close vicinity of the LO-phonon of the undoped material. Although this observation may be a result of an unknown effect, which is beyond our simple dielectric function approach, we speculate it can also be attributed to the appearance of the transverse plasmon-phonon modes in our spectra due to disorder induced breaking of usual selection rules in Raman scattering processes.[11] The effect of the metal-insulator transition induced by the application of the magnetic field is observed with Raman scattering experiments on samples with relatively low electron concentrations. In the insulating state, a repulsion is observed between the intradonor $1s$-$2p$ excitation and the LO-phonon mode, due to the Fröhlich interaction,[12,13] however, the analogous effect involving the cyclotron resonance excitation is not seen in the metallic phase.

Our studies of coupling between the electronic and phonon excitations are complementary to the more common far-infrared absorption investigations of such effects.[12–21] However, the latter experiments probe the transverse plasma excitations which, in addition, are characterized by very small k vectors provided by far infrared light. Raman scattering spectra are sensitive to longitudinal modes and to nonlocal effects (characteristic of excitations with large k vectors), and indeed offer extra information. This has been already shown in the past, though the experiments reported on bulk semiconductors were restricted to relatively low magnetic fields and focused on a nondegenerate, Maxwellian plasma.[22,23] On the other hand, there exist a number of works, concerning both Raman scattering[7,24,25] and far-infrared magnetospectroscopy,[18,21] which address the issue of coupling between the electronic and phonon excitations in two-dimensional semiconductor structures.[21,26] The physics of low energy excitations in these structures is far more complex because of the modification of the energy spectrum due to effects of spatial confinement. An apparent controversy

TABLE I. Characteristic parameters of the investigated samples (at liquid nitrogen temperature). Energy positions of Raman scattering signals due to ω_- and ω_+ coupled plasmon phonon modes and the deduced plasmon frequencies ω_p are listed in columns 2, 3, and 4, respectively. m^* is the estimated effective mass at the Fermi energy, in units of the electron mass. n_0 denotes the nominal electron concentration, whereas n is the concentration value estimated from Raman scattering data (see text).

Sample	ω_- (meV)	ω_+ (meV)	ω_p (meV)	m^*	n (cm^{-3})	n_0 (cm^{-3})
E15/91/1	10	36.7	10.8	0.0675	3.8×10^{16}	5×10^{16}
E2/92/5a	14.2	37.0	15.4	0.0679	1.2×10^{17}	9×10^{16}
B47B	19.6	37.6	21.6	0.0683	2.5×10^{17}	2×10^{17}
B47D	22.4	38.1	25.0	0.0694	3.4×10^{17}	3×10^{17}
B47F	30.6	45.8	41.3	0.0708	9.4×10^{17}	9×10^{17}
B43H	31.8	51.4	48.2	0.0708	1.3×10^{17}	1.1×10^{17}

exists regarding the fundamental problem of Fröhlich interaction: whether it manifests itself as a resonant repulsion between the cyclotron resonance and LO-phononlike modes for a two-dimensional electron gas, or not.[18–21] Our studies of bulk material presented in this paper may help in a better understanding of low dimensional systems.

II. SAMPLE CHARACTERIZATION AND EXPERIMENTAL DETAILS

The *n*-type GaAs samples used for experiments were either bulk GaAs crystals (grown using the conventional Czochralski method) or thin layers (~0.3 mm thick) fabricated using the liquid phase epitaxy technique. No special attention has been paid to the crystallographic orientation of our samples, but presumably, their front surfaces are perpendicular to the (100) axis. The nominal, room temperature electron concentration in these samples range from $n_0 \sim 5\times10^{16}$ cm^{-3} to $\sim10^{18}$ cm^{-3} (see Table I).

The inelastic light scattering (Raman) experiments were performed at liquid nitrogen (T=77 K) and helium (4.2 K) bath temperatures, in a back scattering geometry: the wave vector k_i of the incident light antiparallel to the wave vector k_s of the scattered light. A specially designed fiber optic system, with one fiber for the excitation and the second one for the collection, was used to transmit the unpolarized light to and from the sample immersed in a cryogenic liquid. A tunable Ti:sapphire laser was used as the excitation source, while the signal was dispersed with a triple *XY*-Dilor spectrometer equipped with a CCD camera. Our choice for the laser wavelength was to use below band gap excitation in the range 820–860 nm. Under such conditions the excitation light penetrates a large volume of the crystal and therefore the signals from the surface depletion layer are avoided.

Representative Raman scattering spectra of our samples, measured at 77 K and zero magnetic field are shown in Fig. 1. A very characteristic sharp line observed around 33.75 meV is due to transverse optical (TO) phonons. Although using the back scattering geometry one expects to probe mainly the longitudinal excitations, the observation of the TO-mode is very typical for experiments with below band gap excitation for which the multiple reflections between sample surfaces break the usual selection rules. The energy position of the TO signal is sample independent and insensitive to the magnetic field (as shown below), and this signal will be disregarded in the following. Notably, no signal related to the longitudinal optical (LO) phonons, otherwise typical for undoped crystals, is observed. Instead, each spectrum shows two characteristic features whose energy positions and spectral broadening depend on electron concentration in the sample. These two Raman scattering peaks, denoted as ω_- and ω_+ in Fig. 1, are due to coupled (mixed) plasmon–LO-phonon modes which are inherent to polar materials containing free carriers.[2,7] Distinctively, peaks associated with phononlike modes, close in energy to the LO-phonon of the undoped crystal, are narrower than those related to plasmonlike modes (see Fig. 1). As shown in Fig.

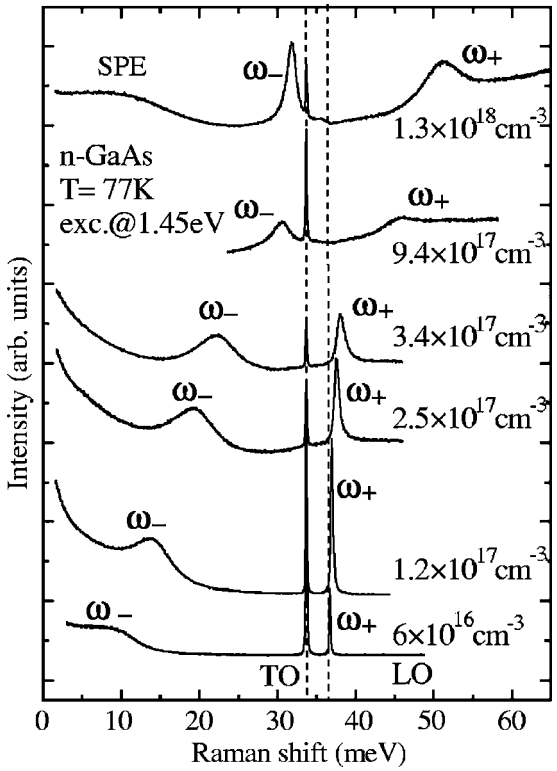

FIG. 1. Raman scattering spectra of the investigated samples, measured in the absence of the magnetic field at liquid nitrogen temperature and laser excitation energy of 1.45 eV.

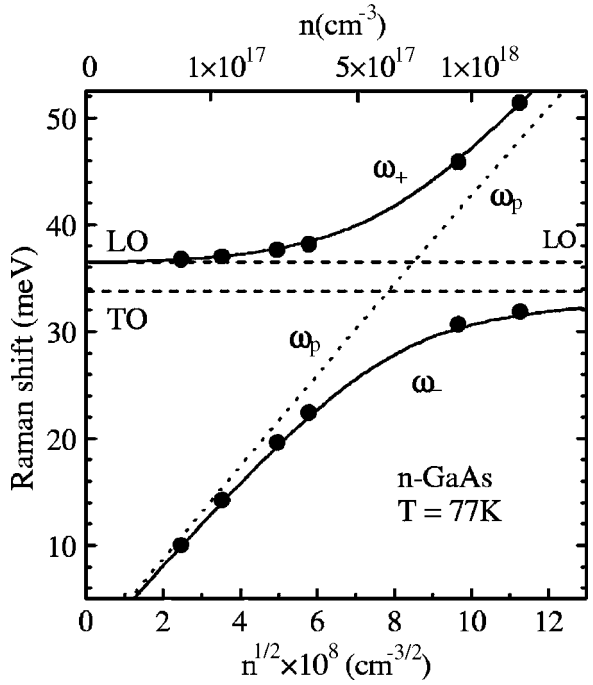

FIG. 2. Peak energies of Raman scattering signal related to coupled plasmon-phonon modes (closed circles), as a function of the electron concentration in the sample. Energies of coupled plasmon-phonon modes are shown with solid lines, whereas the dotted line accounts for the energy of the "bare" plasmon mode, all in the limit of the zero wave vector. Dashed lines represent the LO- and TO-phonon energies of undoped GaAs.

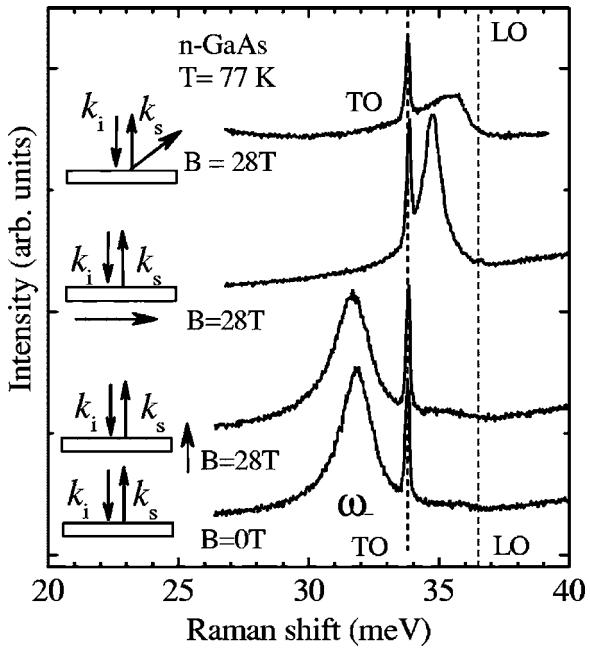

FIG. 3. Raman scattering spectra of the sample with $n=1.3\times10^{18}$cm^{-3} measured at high magnetic field in Faraday, Voigt, and oblique angle configurations. The zero field spectrum (bottom trace) is shown for comparison.

2, the energy position of these peaks shows a characteristic dependence on the electron concentration in the sample.

In a rough approximation, when considering only the modes with zero wave vector, the frequencies of coupled plasmon–LO-phonon modes are the solutions of the expression setting the dispersionless dielectric function $\epsilon(\omega)$ to zero (Ref. 2).

$$\epsilon(\omega) = \epsilon_\infty \frac{\omega^2 - \omega_{\mathrm{LO}}{}^2}{\omega^2 - \omega_{\mathrm{TO}}{}^2} - \epsilon_\infty \frac{\omega_p{}^2}{\omega^2} = 0. \quad (1)$$

Here, ϵ_∞ is the high frequency dielectric constant, ω_{LO} and ω_{TO} stand for longitudinal and transverse optical phonon frequency, respectively, and $\omega_p=(ne^2/\epsilon_0\epsilon_\infty m^*)^{1/2}$ denotes the "bare" plasmon frequency [m^* is the electron effective mass (at the Fermi energy) and n denotes the electron concentration]. Two solutions $\omega_\pm$ of the above equation (Ref. 2):

$$\omega_\pm = \frac{1}{2}\sqrt{\omega_p{}^2 + \omega_{\mathrm{LO}}{}^2 \pm [(\omega_p{}^2 + \omega_{\mathrm{LO}}{}^2)^2 - 4\omega_p{}^2\omega_{\mathrm{TO}}{}^2]^{1/2}} \quad (2)$$

define the $k=0$ frequencies of coupled plasmon–LO-phonon modes. The calculated energies of ω_- and ω_+ modes for different electron concentrations n are shown in Fig. 2 with solid lines, assuming 36.5 and 33.75 meV for LO- and TO-phonon energies, respectively. The dotted line in this figure shows the energy of the bare plasmon mode ω_p, which would be a linear function of $n^{1/2}$, if not for a nonparabolicity effect[27] which we have included in the calculations. The experimental data are also shown in this figure. For each spectrum shown in Fig. 1 we have read the energies of the ω_- and ω_+ Raman peaks and brought each pair of these experimental values (denoted with solid dots) on the calculated ω_- and ω_+ curves. In this way, the electron concentration has been readjusted for each sample. As can be seen in Table I, these electron concentrations n, to which we refer further, coincide fairly well with the corresponding nominal values. It is worth noticing that the ω_-, ω_+, and ω_p frequencies satisfy a simple relation:

$$(ne^2/\epsilon_0\epsilon_\infty m^*)^{1/2} = \omega_p = \sqrt{\omega_+{}^2 + \omega_-{}^2 - \omega_{\mathrm{LO}}{}^2}. \quad (3)$$

In a simple approximation, (if the effective mass is known and does not depend on the electron concentration, i.e., the effect of nonparabolicity is neglected), a knowledge of the energies of ω_- and ω_+ modes provides a very direct estimate of the electron concentration in the sample.

Magnetic field experiments were carried out using a resistive magnet supplying fields up to 28 T. Spectra were measured for three different configurations of the magnetic field: Faraday ($k_s \| \vec{B}$), Voigt ($k_s \perp \vec{B}$), and the so-called oblique configuration $\angle(k_s, \vec{B})=45°$. The overall effect of the magnetic field on Raman scattering spectra of coupled plasmon–LO-phonon modes measured for three different configurations is illustrated in Fig. 3. The application of the magnetic field induces noticeable changes in the spectra for Voigt and oblique configurations but scarcely affects those measured in the Faraday configuration. This is to be expected for our backscattering experiments as they predominantly probe the longitudinal excitations which remain unchanged when

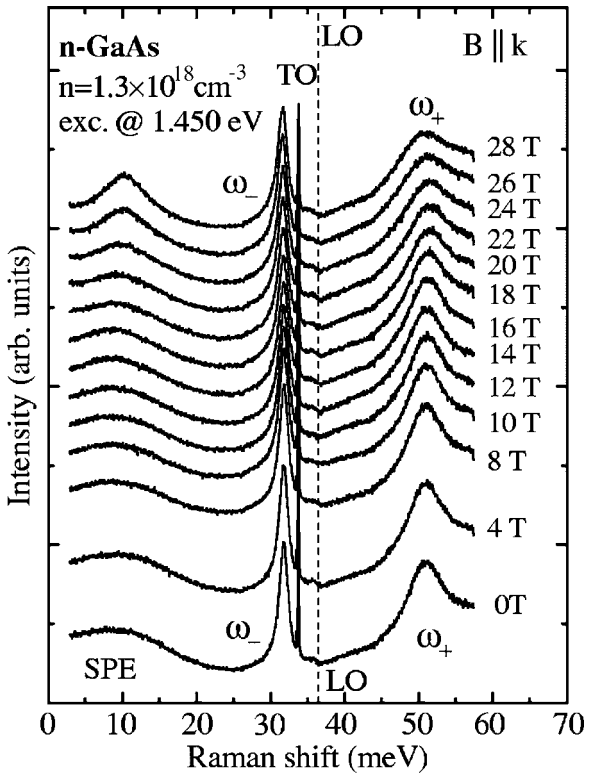

FIG. 4. Magnetic field evolution of Raman scattering spectra measured in the Faraday configuration for the sample with the highest electron concentration.

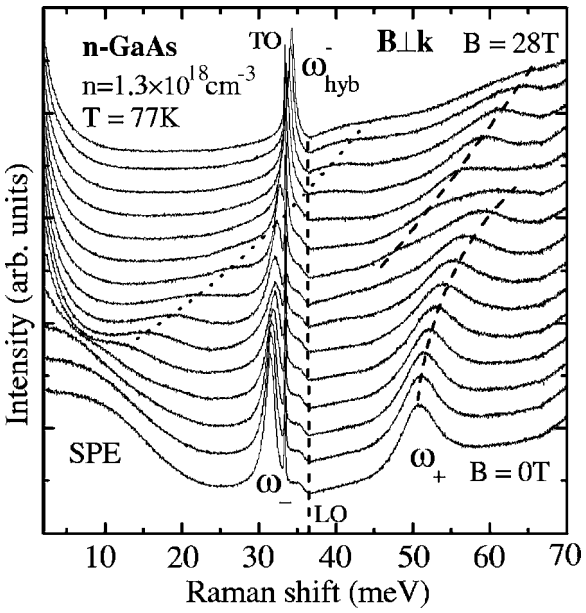

FIG. 5. Magnetic field evolution of Raman scattering spectra measured in Voigt configuration for the sample with the highest electron concentration.

propagating along the magnetic field but are clearly modified in other configurations, which simply reflects the character of the Lorentz force.

III. HIGH ELECTRON CONCENTRATION LIMIT

The Raman spectra measured versus magnetic field for the sample with the highest electron concentration are shown in Figs. 4–6.

We notice again the small changes in the spectra measured in the Faraday configuration but notable spectral evolution with the magnetic field for the Voigt as well as the oblique configuration. Although our attention is mostly focused on the investigation of collective modes we also note the observation of a broad, low-energy signal, denoted as single particle excitations (SPE) in the spectra at zero magnetic field. We think this signal is due to single particle excitations of the electron gas. The detailed discussion of this feature and its changes with the magnetic field is beyond the scope of this paper. We mention here, however, its characteristic narrowing with the magnetic field in the Faraday configuration, its possible emergence into the cyclotron resonance mode observed in the Voigt configuration, and complex evolution in the oblique configuration. Except for the sharp signal due to the TO-phonon, insensitive to the magnetic field, all other observed Raman peaks are assumed to reflect the magnetic field evolution of the collective, plasmon–LO-phonon modes. As shown below, these are predominantly the longitudinal coupled plasmon–LO-phonon modes which we observe for the sample with the highest electron concentration, as generally expected for the backscattering experiments.

In calculations we assume the magnetic field vector in the z-direction $\vec{B}=(0,0,B)$, consider the dielectric tensor in its standard form:

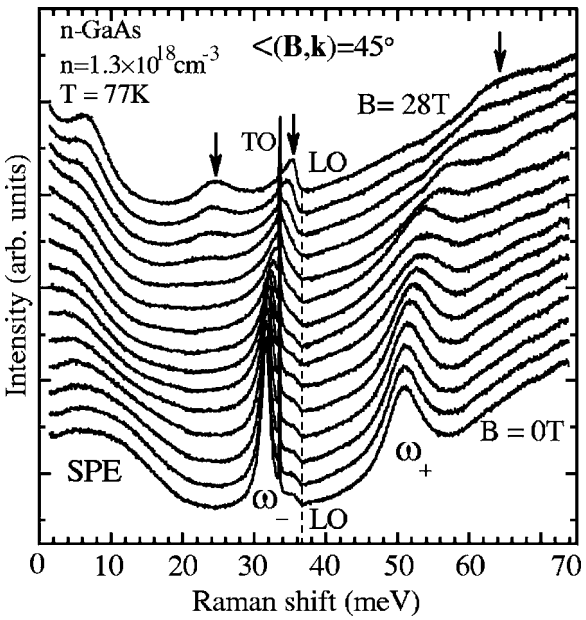

FIG. 6. Magnetic field evolution of Raman scattering spectra measured in the oblique geometry configuration for the sample with the highest electron concentration.

$$\hat{\varepsilon} = \begin{pmatrix} \varepsilon_{xx} & \varepsilon_{xy} & 0 \\ -\varepsilon_{xy} & \varepsilon_{xx} & 0 \\ 0 & 0 & \varepsilon_{zz} \end{pmatrix} \tag{4}$$

and search for frequencies of the longitudinal coupled plasmon–LO-phonon modes, in a given configuration, by solving the following equation (Ref. 1)

$$\vec{k}\hat{\varepsilon}\vec{k} = 0. \tag{5}$$

Here, the direction of the propagating mode is defined by its wave vector $\vec{k}$; $\vec{k} \sim (0,0,1)$, $\vec{k} \sim (0,1,0)$, and $\vec{k} \sim (0,1,1)$, correspondingly, for Faraday, Voigt, and the oblique configuration.

We first continue to consider the dielectric response in the limit of zero wave vectors (the so-called local approximation). In this case the dielectric tensor components can be written as follows:

$$\varepsilon_{xx} = \epsilon_\infty \frac{\omega^2 - \omega_{\mathrm{LO}}{}^2}{\omega^2 - \omega_{\mathrm{TO}}{}^2} - \epsilon_\infty \frac{\omega_p{}^2}{\omega^2 - \omega_c{}^2}, \tag{6}$$

$$\varepsilon_{xy} = i \frac{\omega_c}{\omega} \frac{\varepsilon_\infty \omega_p^2}{\omega^2 - \omega_c^2}, \tag{7}$$

and

$$\varepsilon_{zz} = \epsilon_\infty \frac{\omega^2 - \omega_{\mathrm{LO}}{}^2}{\omega^2 - \omega_{\mathrm{TO}}{}^2} - \epsilon_\infty \frac{\omega_p{}^2}{\omega^2}, \tag{8}$$

where $\omega_c = eB/m^*$ stands for the electron cyclotron frequency.

Considering the Faraday configuration we now explicitly see that equation $\varepsilon_{zz}=0$, which as a matter of fact is identical to Eq. (1), does not include the magnetic field as a parameter. Therefore, the longitudinal modes are not affected by the magnetic field for this particular configuration, in agreement with the experimental data (see Fig. 7). A search for the frequencies of longitudinal modes in the Voigt configuration implies seeking the solutions for $\varepsilon_{xx}=0$, which are nontrivial and customarily referred to as the hybrid modes:

$$\omega_{hyb}^{\pm} = \left(\frac{\Omega_c^2 + \omega_{\mathrm{LO}}^2}{2} \pm \frac{1}{2} \sqrt{(\Omega_c^2 + \omega_{\mathrm{LO}}^2)^2 - 4(\omega_c^2 \omega_{\mathrm{LO}}^2 + \omega_p^2 \omega_{\mathrm{TO}}^2)} \right)^{1/2}. \tag{9}$$

Here, $\Omega_c^2 = \omega_c^2 + \omega_p^2$ denotes the square of the bare magnetoplasma frequency. $\omega_{hyb}^{+} \to \omega_+$ and $\omega_{hyb}^{-} \to \omega_-$ when the magnetic field tends to zero, whereas $\omega_{hyb}^{+} \to \omega_c$ and $\omega_{hyb}^{-} \to \omega_{\mathrm{LO}}$ in the high field limit. The energies of these hybrid modes calculated as a function of the magnetic field for the sample with the highest electron concentration are shown in Fig. 8 with dotted lines. They roughly reproduce the experimental data but clearly disregard the anticrossing type effect which is particularly pronounced for the ω_{hyb}^{+} mode in the vicinity of 18 T in this particular sample. The latter effect is beyond the local approximation which we are considering up to now. Nevertheless, this simple approximation remains sufficient to describe our observation in the oblique configuration. The calculated solutions of the equation $\varepsilon_{xx}+\varepsilon_{zz}=0$ shown in Fig. 9 with solid lines satisfactorily reproduce the experimental data.

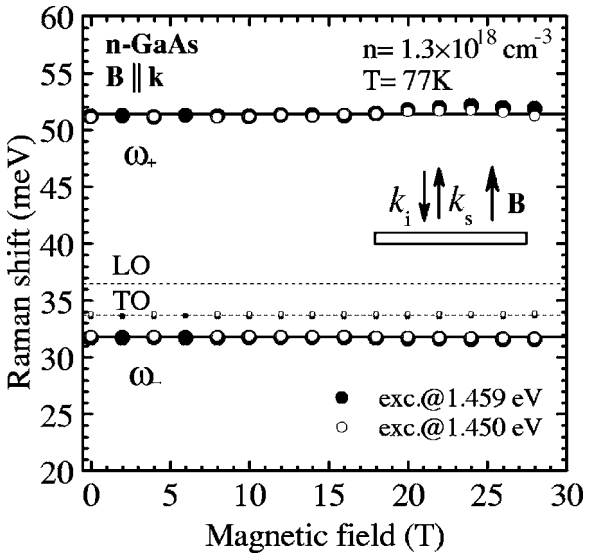

FIG. 7. Magnetic field dependence of energy positions of Raman scattering peaks measured in the Faraday configuration for the sample with the highest electron concentration.

In order to account for the nonlocal effects, which are clearly observed in Voigt-configuration experiments, the dispersion of the dielectric response has to be taken into account. Considering the case of a degenerate electron gas in our high concentration samples ($n \geqslant 3.4 \times 10^{17}$ cm^{-3}, and

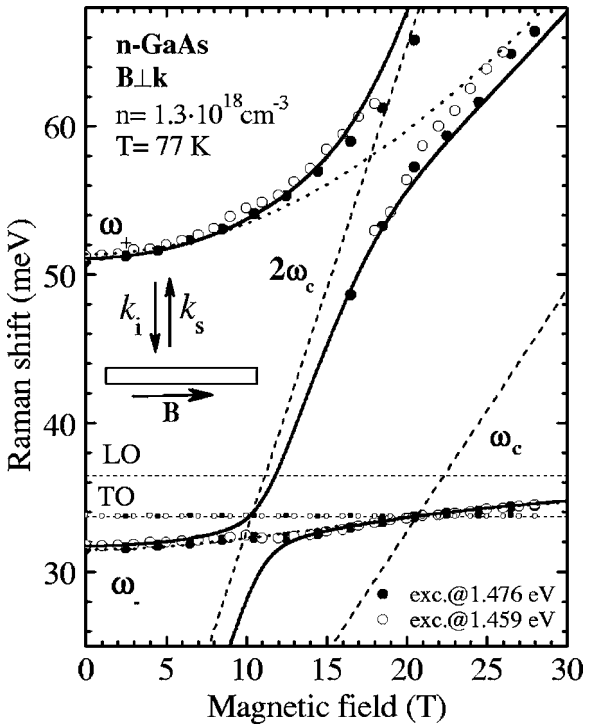

FIG. 8. Magnetic field dependence of energy positions of Raman scattering peaks measured in the Voigt configuration for the sample with the highest electron concentration.

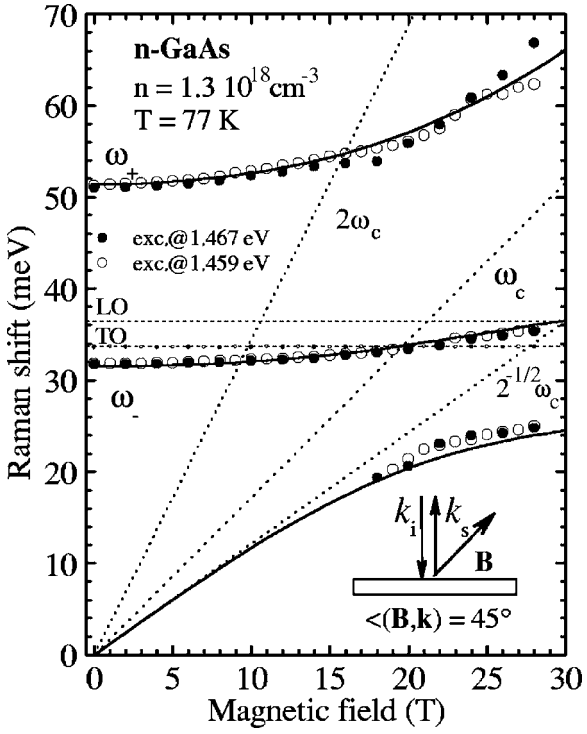

FIG. 9. Magnetic field dependence of energy positions of Raman scattering peaks measured in the oblique geometry configuration for the sample with the highest electron concentration.

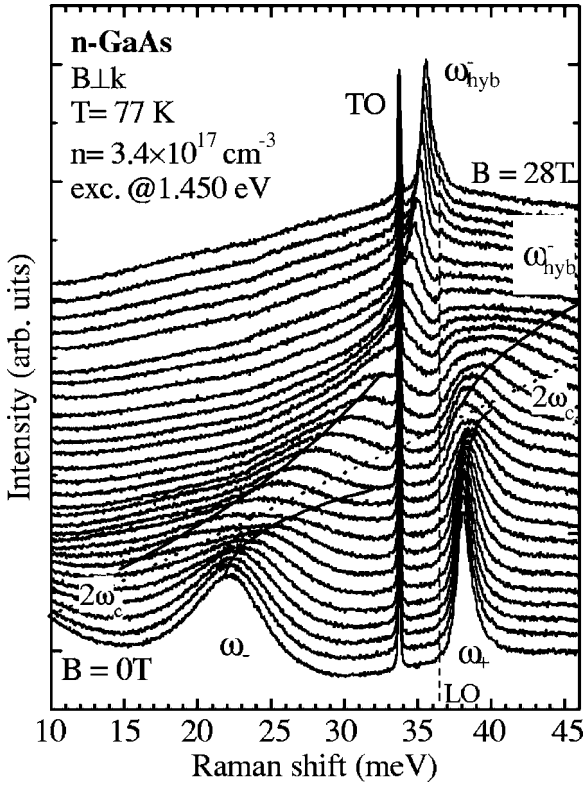

FIG. 10. Raman scattering spectra measured in Voigt geometry for a sample with $n=3.4\times10^{17}$ cm^{-3}.

therefore $E_F/kT \geqslant 4$ for $T \leqslant 78$ K) we assume that

$$\varepsilon_{xx} = \epsilon_\infty \frac{\omega^2 - \omega_{\mathrm{LO}}{}^2}{\omega^2 - \omega_{\mathrm{TO}}{}^2} - \epsilon_\infty \omega_p{}^2 \left(\frac{1-\lambda^2}{\omega^2 - \omega_c{}^2} + \frac{\lambda}{\omega^2 - 4\omega_c} \right), \tag{10}$$

where $\lambda = \frac{k^2}{\omega_c}\langle v^2 \rangle$ is a measure of nonlocality and the mean square velocity for the degenerate electron gas is $\langle v^2 \rangle = 6E_F/5m^*$, where E_F stands for the Fermi energy (at zero temperature). Strictly speaking, Eq. (10) has been derived[1,23] for Maxwellian (nondegenerate) plasmas for which $\langle v^2 \rangle = 3kT/m^*$. Our approach to simulate the experimental data is to use Eq. (10) also in the case of a degenerate gas, with an accordingly modified expression for $\langle v^2 \rangle$. For a given excitation wavelength λ_L used in our backscattering experiments the momentum transfer is $k = 4\pi n_L/\lambda_L \approx 5\times10^7$ cm^{-1}.

Again, the solutions of $\varepsilon_{xx}=0$ yield the magnetic field evolution of the frequency of the longitudinal plasmon-phonon modes observed in the Voigt geometry, this time, however, the modes with a nonzero wave vector are investigated. Solid lines in Fig. 8 represent the results of these calculations for the sample with highest electron concentration. Analogous data obtained from spectra measured for a sample with slightly lower concentration (see Fig. 10) are shown in Fig. 11. Modes with finite k have frequencies higher than those with $k=0$ and therefore fitting the data within the nonlocal approximation requires the readjustment (reduction) of the electron concentration. Whereas the local approximation yields $n=1.3\times10^{18}$ cm^{-3} and $n=3.4\times10^{17}$ cm^{-3} in our two, high concentration samples, the readjusted values within the nonlocal approach are $n=1.1\times10^{18}$ cm^{-3} and $n=3.2\times10^{17}$ cm^{-3}, respectively. Considering the $k\neq0$ excitations we uncover a significant result which is that finite wave vector collective hybrid modes interact with collective, cyclotron excitations with a frequency of $2\omega_c$ (Bernstein modes). These Bernstein modes are usually inactive in Raman scattering experiments on three-

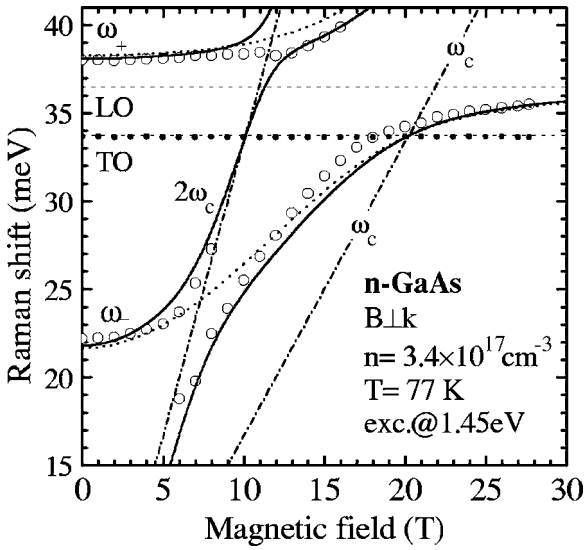

FIG. 11. Magnetic field dependence of energy positions of Raman scattering peaks measured in Voigt geometry for a sample with $n=3.4\times10^{17}$ cm^{-3}.

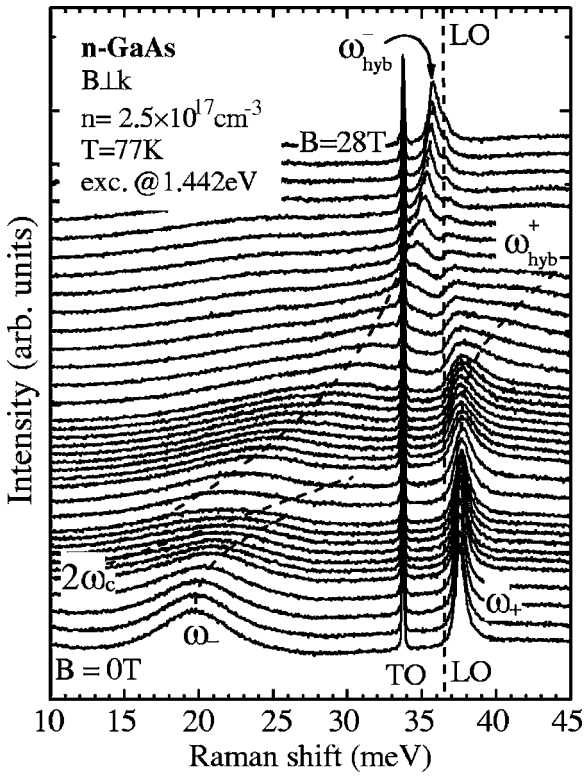

FIG. 12. Voigt configuration Raman scattering spectra measured as a function of the magnetic field at $T=77$ K for a sample with $n=2.5\times10^{17}$ cm^{-3}.

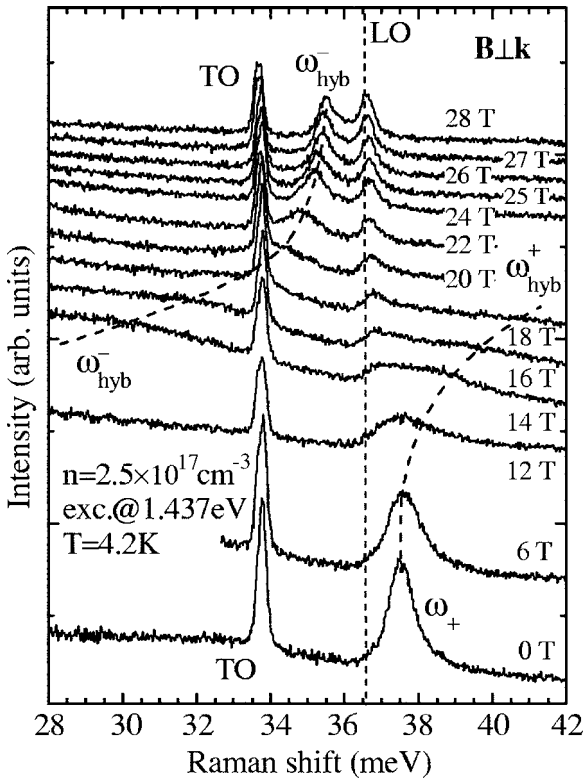

FIG. 13. Voigt configuration Raman scattering spectra measured as a function of the magnetic field at $T=4.2$ K for a sample with $n=2.5\times10^{17}$ cm^{-3}.

dimensional (3D) plasmas[28] except the anticrossing region when they couple with hybrid magneto plasmon modes.[23] As can be seen in Figs. 8 and 11, Bernstein modes predominantly couple with plasmonlike modes and less efficiently with phononlike modes. This is seen clearly in the experiments and well reproduced in the calculations. The plasmonlike character dominates the ω_+ mode in high concentration samples and the ω_- mode in low concentration samples. Accordingly, Bernstein modes effectively interact with the ω_+ mode in the sample with $n=1.3\times10^{18}$ cm^{-3} but predominantly couple to the ω_- mode in the sample with $n=3.4\times10^{17}$ cm^{-3}. Interactions with phononlike modes (i.e., ω_- and ω_+ correspondingly for samples with $n=1.3\times10^{18}$ cm^{-3} and $n=3.4\times10^{17}$ cm^{-3}) are considerably weaker but still marked in the experiment, though only in the form of broadening of the Raman scattering signal. Concluding this section, we note that the standard approach of the dielectric function, which was developed for the case of classical magnetoplasmas, accounts well for our experimental results even in the limit of high magnetic fields. However, as will be discussed later, some disagreement progressively appears when samples with lower electron concentrations are considered.

IV. INTERMEDIATE ELECTRON CONCENTRATIONS

Figures 12 and 13 illustrate the Raman scattering spectra measured in a Voigt configuration on the sample with lower electron concentration ($n=2.5\times10^{17}$ cm^{-3}), correspondingly, at $T=77$ K and $T=4.2$ K. The characteristic longitudinal plasmon-phonon excitations can still be recognized in these: the ω^-_{hyb} mode is particularly well pronounced at high magnetic fields. The data are more clear at $T=77$ K than at $T=4.2$ K because strong luminescence at low temperatures in this sample overlaps with the Raman scattering signal. The prominent feature present in these data is an additional, very characteristic, Raman scattering peak which develops from the low energy wing of the ω_+ mode and approaches, at high magnetic fields, the expected position of the LO mode of an undoped crystal. The traces of this effect can be found even in the previously discussed data on the sample with higher electron concentration (see Fig. 10). It appears to be more clear at lower electron concentrations and is particularly well pronounced in the low temperature data (Figs. 12 and 13). Within the standard approach presented in the preceding section, this additional Raman scattering signal cannot be attributed to any longitudinal magnetoplasmon-phonon mode of the doped material. Although one could question the validity of the conventional dielectric function approach to explain the high field data, we think that there are more conventional reasons that possibly account for the observed effect. We may consider two scenarios depending on the way one sees the field evolution of the additional Raman scattering signal. As a matter of fact, the experimental data do not allow us to definitely distinguish whether the appearance of the additional Raman scattering peak should be seen as a development, at high magnetic fields, of the signal corresponding to the LO mode of the undoped material, or whether this peak

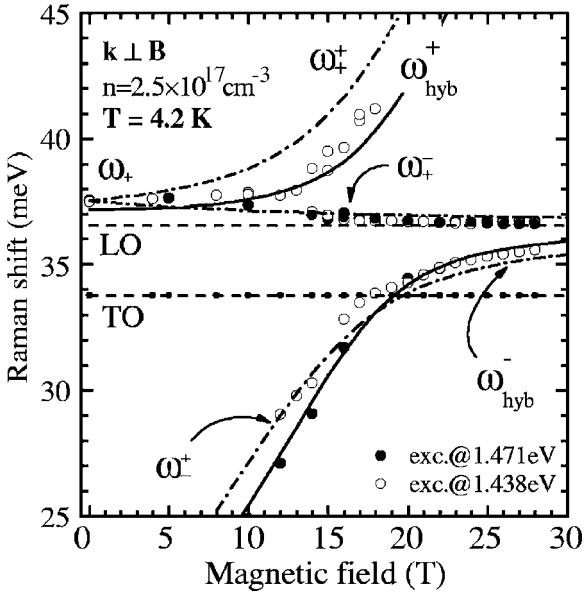

FIG. 14. Magnetic field dependence of peak positions of Raman scattering signal measured in Voigt configuration at $T=4.2$ K for a sample with $n=2.5\times10^{17}$ cm^{-3}.

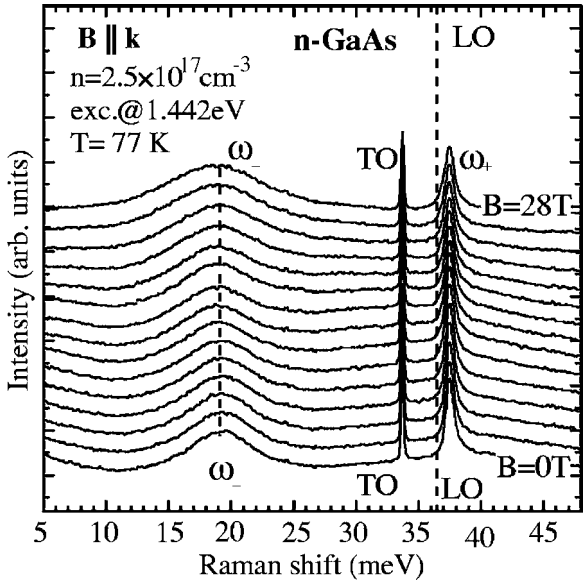

FIG. 15. Magnetic field dependence of peak positions of Raman scattering signal measured in Faraday configuration at $T=77$ K for a sample with $n=2.5\times10^{17}$ cm^{-3}.

emerges from the ω_+ mode and its energy position weakly decreases as a function of the magnetic field. Considering the former viewpoint one tends to consider a possible effect of the decrease of the electron concentration as a function of the magnetic field and/or temperature (effect of magnetic and/or temperature free out). It will be shown in the next section that such an effect can indeed be important in the case of samples with still smaller electron concentrations; however, it is unlikely to play a role in the case of the present sample. It can be clearly seen in Figs. 12 and 13 that the additional high field Raman scattering signal (around the LO frequency of the undoped material) is simultaneously observed together with the ω_{hyb}^- peak whose appearance is a clear signature of the presence of free electrons in the sample. This ω_{hyb}^- mode can be followed as a function of the magnetic field and for two different temperatures and its behavior does not indicate any field or temperature changes of the electron concentration in the sample.[29,30] The alternative explanation, which we think is more probable, is to assign this signal to one of the possible components of the transverse plasmon-phonon mode. After all, the observation of any transverse modes in our below-band gap excitation experiments should not be so surprising as the TO-phonon mode always contributes to the measured Raman scattering spectra. Figure 14 illustrates the collection of the data regarding the magnetic field dependence of energy positions of Raman scattering peaks measured at $T=4.2$ K in Voigt geometry on the sample with $n=2.5\times10^{17}$ cm^{-3}. Solid lines in this figure denote the calculated energies of the longitudinal hybrid plasmon-phonon modes whereas dashed-dotted lines are the calculated positions of the transverse modes. The local approximation has been used for the sake of simplicity. Frequencies of the transverse modes have been derived in a conventional way by finding the singularities of the dielectric function given by (Refs. 15 and 16)

$$\varepsilon(\omega)=\frac{2\varepsilon_r\varepsilon_l}{\varepsilon_r+\varepsilon_l} \tag{11}$$

in which

$$\varepsilon_{r,l}=\epsilon_\infty\left[1+\frac{\omega_{\mathrm{LO}}^2-\omega_{\mathrm{TO}}{}^2}{\omega_{\mathrm{TO}}^2-\omega^2}-\frac{\omega_p{}^2}{\omega(\omega\pm\omega_c)}\right] \tag{12}$$

accounts for the right $(r,+)$ and left $(1,-)$ circularly polarized waves. As can be seen again in Fig. 14, the additional Raman signal observed in the vicinity of the undressed LO-phonon mode cannot be assigned to any longitudinal plasmon-phonon mode. However, its energy position coincides quite well with the expected position of the ω_+^- component of the transverse ω_+ mode.

The observation of the transverse modes should not in principle be specific for the Voigt configuration of the experimental arrangement. The spectra measured for the sample with $n=2.5\times10^{17}$ cm^{-3} but in the Faraday configuration are shown in Figs. 15 and 16. Inspecting these data, we find hardly any traces of an additional, near LO-phonon Raman scattering signal in the spectra measured at $T=77$ K but find it clearly in the results obtained at $T=4.2$ K, i.e., under conditions when this peak is also well pronounced in Voigt configuration spectra.

Identifying the additional Raman mode with the transverse excitation of the plasmon-phonon mode we note that its appearance is favored in samples with lower electron concentrations, at low temperatures and in high magnetic fields. The mechanism that breaks the usual selection rules and allows the observation of the transverse plasmon-phonon modes is not completely clear for us but we think it is related to disorder. Taking, for example, the electron mobility as a measure of the disorder in our sample we expect it to be lower at low temperatures and in low concentration samples.

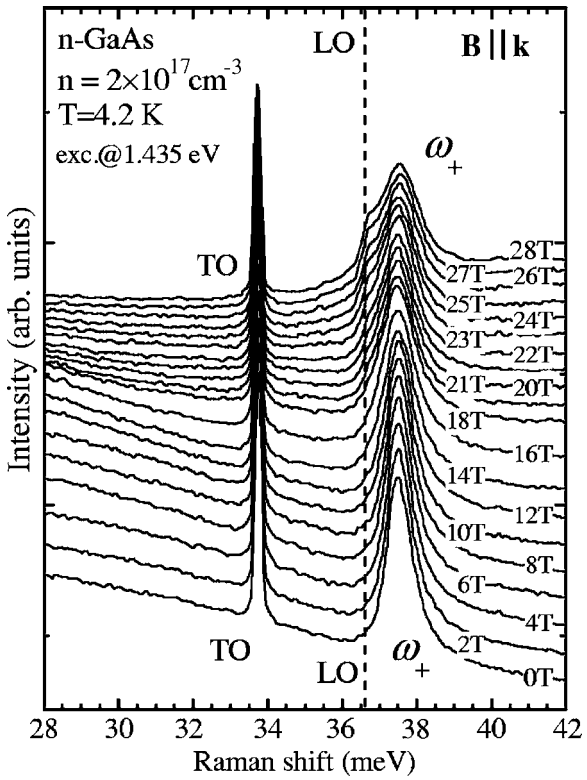

FIG. 16. Magnetic field dependence of peak positions of Raman scattering signal measured in Faraday configuration at $T=4.2$ K for a sample with $n=2.5\times10^{17}$ cm^{-3}.

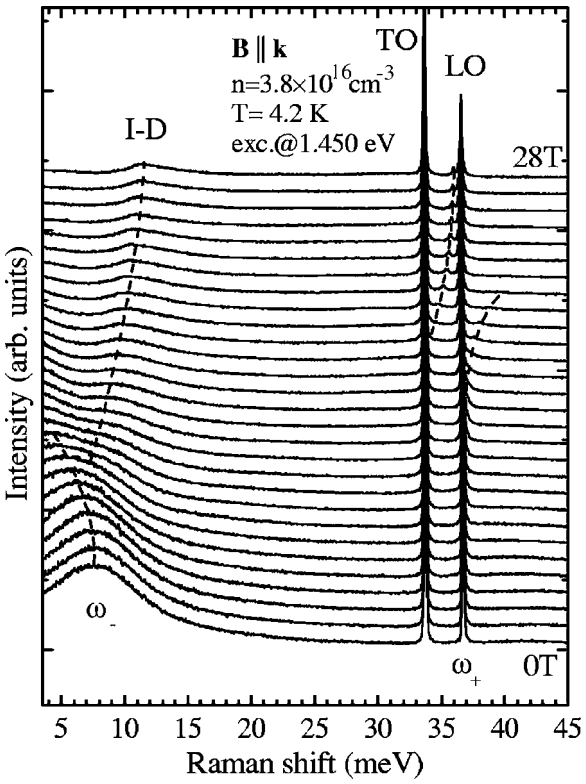

FIG. 17. Magnetic field evolution of Raman scattering spectra measured in Faraday configuration at $T=4.2$ K for a sample with $n=3.8\times10^{16}$ cm^{-3}.

One may also speculate about an effect of the magnetic field induced disorder. Field induced broadening of peaks related to plasmon-phonon modes measured in the Faraday configuration, which can be seen, for example, in Fig. 15, could be an indication of such an effect. It might also be that significant broadening of the Raman scattering signal seen in Fig. 13 above the LO-phonon energy for intermediate magnetic fields (16–18 T) is due to disorder activated continuum of excitations with different wave vectors.

Firm conclusions regarding the identification of the additional Raman scattering signal near LO-phonon energy in our samples with lower electron concentration can be, however, drawn only together with theoretical work, which is beyond the scope of this paper. Breaking of the usual selection rules in Raman scattering experiments, which often allow one to observe transverse modes, seems to be an important and poorly understood effect.[11] Possible limitations of the classical dielectric function approach that we use to describe our data are also not clear.

V. MAGNETIC FIELD INDUCED METAL-INSULATOR TRANSITION

Our lowest concentration samples show a quantitatively different behavior, particularly when measured at low temperatures. Here we consider the results for sample E15/91/1, which in contrast to all other investigated samples, shows changes in the electron concentration as a function of temperature, from $n\sim6\times10^{16}$ cm^{-3} at $T=77$ K to $n\sim3.8\times10^{16}$ cm^{-3} at $T=4.2$ K, as could be estimated from the measured energy position of coupled plasmon-phonon modes. To demonstrate the characteristic behavior in the low concentration limit we focus on the results obtained on this sample in Faraday configuration measurements at $T=4.2$ K. The representative spectra are shown in Fig. 17. The zoomed part of these spectra in a range around the energy of the undressed LO-phonon is illustrated in Fig. 18. In this sample, the magnetic field noticeably affects the Faraday configura-

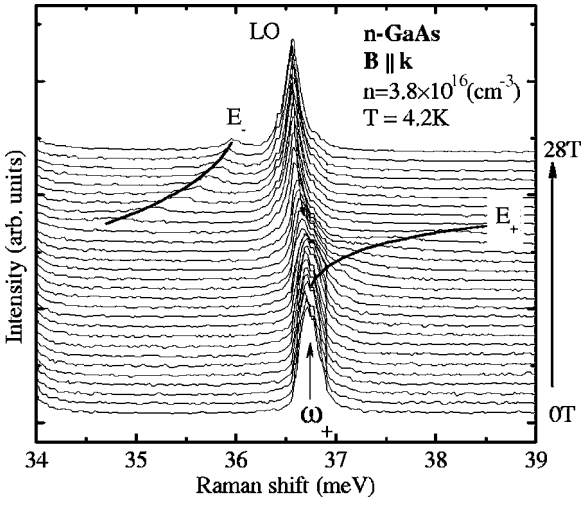

FIG. 18. The zoom of the data from Fig. 17 in the range around LO-phonon.

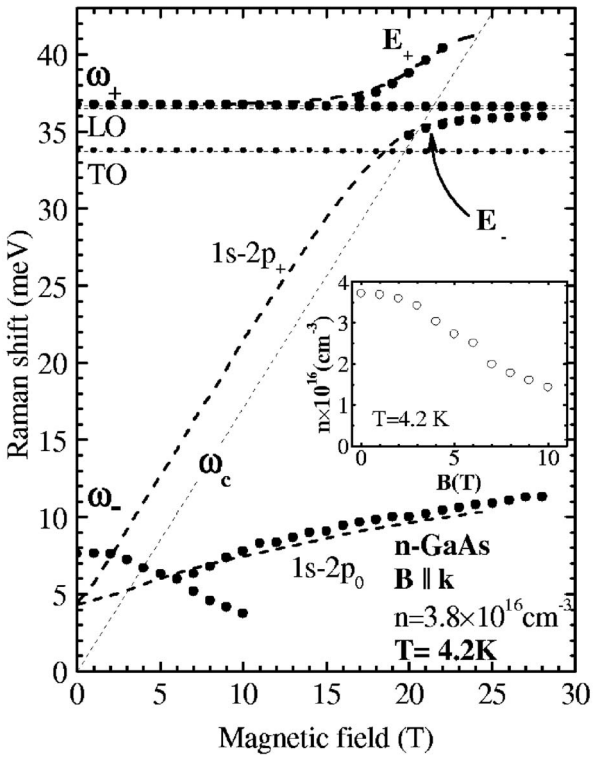

FIG. 19. Magnetic field dependence of peak positions of Raman scattering signal measured in Faraday configuration at $T=4.2$ K for a sample with $n=3.8\times10^{16}$ cm^{-3}.

tion spectra, in contrast to the case of previously discussed results for samples with a higher electron concentration. The characteristic ω_- and ω_+ plasmon-phonon modes are still well defined in the spectra measured at zero magnetic field. However, both ω_- and ω_+ peaks shift toward lower energies, progressively when the magnetic field is applied. The energy of ω_- tends to decrease to zero and merges with the laser line position whereas ω_+ approaches the position of the undressed LO-phonon line at sufficiently high magnetic fields. In addition, new signals appear at high magnetic fields: one in the low energy part of the spectra denoted as *I-D* in Fig. 17 and two others, E_+ and E_- in the vicinity of the LO-phonon peak. The evolution of the energy positions of the measured Raman scattering signals versus magnetic field is shown in detail in Fig. 19. The appearance of the effect of the magnetic field freeze out (decrease of the electron concentration as a function of the magnetic field and in consequence the field induced metal-insulator transition) is our essential conjecture to interpret these data. The electron concentration can be reasonably well monitored by the position of the ω_- peak, and the estimated changes of n as a function of the magnetic field are shown in the inset to Fig. 19. The logical consequence of the freezing of electrons on donor sites is a possible appearance of Raman signal related to intradonor transitions. The additional transitions which are observed in the spectra at high magnetic field are therefore attributed to Raman scattering signals related to the excitations between the $1s$ ground state and the excited states of electrons frozen on donor states. The *I-D* line is assigned to the $1s$-$2p_0$ transition, which is active in Raman scattering processes and usually observed in experiments on insulating n-type semiconductors. The E_+ and E_- peaks are likely the remnants of signals associated with the $1s$-$2p_+$ transition in the region where it splits due to the resonant magnetopolaron effect. Usually, the $1s$-$2p_+$ transition does not contribute to the Raman scattering signal, but presumably it becomes active when mixed with the LO-phonon mode due to the Fröhlich interaction. Both $1s$-$2p_+$ and $1s$-$2p_0$ transitions can be, however, investigated in far-infrared magnetoabsorption experiments, in a wide range of magnetic fields.[12] In Fig. 19 we compare the positions of the $1s$-$2p_+$ and $1s$-$2p_0$ transitions measured in our Raman scattering experiments with those reported previously from far-infrared absorption studies on n-type GaAs. Dashed lines in this figure represent the overlapping theoretical and experimental results which have been digitized from Ref. 12 (Fig. 3). These lines also coincide well with the data reported here, what is in favor of our interpretation of the present Raman scattering results.

It is worth noticing that, similar to far-infrared magnetoabsorption experiments on different n-type semiconductor structures, we observe the effect of resonant magnetopolaron coupling when electrons are bound to donors (interaction between $1s$-$2p_+$ and LO-phonon excitations), but see hardly any traces of resonant Fröhlich interaction in the metallic phase, between the cyclotron-resonance and any other LO-phononlike modes. Our observations may also give some additional insight into the physics of the resonant magnetopolaron effect, which has been recently reviewed in two-dimensional systems.[18–21,31–33] Besides, our results show an interesting possibility of tracing the metal-insulator transition in n-type semiconductors using Raman scattering experiments.

VI. CONCLUSIONS

We have studied the Raman scattering response of n-type GaAs samples in a wide range of applied magnetic fields, including the yet unexplored high field limit. The prominent features of the measured spectra are due to coupled plasmon-phonon modes. In samples with the highest electron concentration the observed evolution of Raman scattering spectra with the magnetic field is consistent with a classical approach which implies the observation of longitudinal plasmon-phonon excitations. The interaction between Bernstein and plasmon-phonon modes has been clearly observed, and as expected is more or less pronounced when involving modes with plasmon- or phononlike character, respectively. The conventional understanding of high field Raman scattering spectra breaks down in samples with progressively lower electron concentration. The first effect of lowering electron concentration is the appearance, at high magnetic fields, of a Raman scattering signal in a very close vicinity of the LO-phonon of the undoped material. Our tentative interpretation is to assign this peak as due to a disorder activated transverse plasmon-phonon excitation. More speculative explanations are not excluded, but require a rigorous theoretical treatment

of Raman scattering response in the limit of high magnetic fields. The field induced metal-insulator transition is reflected in Raman scattering experiments on samples with the lowest electron concentrations. The plasmon-phonon modes characteristic of the metallic state are replaced by intradonor excitations in the case of the insulating state. The resonant magnetopolaron effect reflecting the interaction between the LO-phonon and the $1s$-$2p$ intradonor excitation is observed in the insulating state but no coupling between LO-phonon and cyclotron resonance excitations is seen in the metallic state.

The authors are grateful to M.L. Sadowski for valuable discussions. A. Wysmolek is grateful for the financial support from the Alexander von Humboldt Foundation. The experiments have been supported in part by the E.C.RITA-CT-2003-505474 Grant.

[1] P. M. Platzman and P. A. Wolff, *Waves and Interactions in Solid State Plasmas* (Academic Press, New York, 1973).
[2] B. B. Varga, Phys. Rev. **137**, A1896 (1965).
[3] A. Mooradian and G. B. Wright, Phys. Rev. Lett. **16**, 999 (1966).
[4] A. Pinczuk, G. Abstreiter, R. Trommer, and M. Cardona, Solid State Commun. **21**, 959 (1977).
[5] G. Abstreiter, R. Trommer, M. Cardona, and A. Pinczuk, Solid State Commun. **30**, 703 (1979).
[6] U. Nowak, W. Richter, and G. Sachs, Phys. Status Solidi B **108**, 131 (1981).
[7] G. Abstreiter, M. Cardona, and A. Pinczuk: *Light Scattering in Solids IV*, edited by M. Cardona and G. Guntherodt (Springer-Verlag, Berlin, 1984).
[8] P. M. Platzman, P. A. Wolff, and N. Tzoar, Phys. Rev. **174**, 489 (1968).
[9] B. Lax, J. Phys. Soc. Jpn. **21**, 165 (1966).
[10] I. B. Bernstein, Phys. Rev. **109**, 10 (1958).
[11] A disorder induced breaking of usual selection rules in Raman scattering process has been particularly discussed in the context of experiments on a two-dimensional electron gas. See, for example, A. Pinczuk, J. P. Valladares, D. Heiman, A. C. Gossard, J. H. English, C. W. Tu, L. Pfeiffer, and K. West, Phys. Rev. Lett. **61**, 2701 (1998); I. K. Marmorkos and S. Das Sarma, Phys. Rev. B **45**, 13396 (1992).
[12] J. P. Cheng, B. D. McCombe, J. M. Shi, F. M. Peeters, and J. T. Devreese, Phys. Rev. B **48**, 7910 (1993).
[13] M. Grynberg, S. Huant, G. Martinez, J. Kossut, T. Wojtowicz, G. Karczewski, J. M. Shi, F. M. Peeters, and J. T. Devreese, Phys. Rev. B **54**, 1467 (1996).
[14] R. Kaplan, E. D. Palik, R. F. Wallis, S. Iwasa, E. Burstein, and Y. Sawada, Phys. Rev. Lett. **18**, 159 (1967).
[15] S. Ivasa, in *Physics of Solids in Intense Magnetic Fields*, edited by E. D. Haidemenakis (Plenum Press, New York 1969), p. 126.
[16] I. Yokota, J. Phys. Soc. Jpn. **21**, 738 (1966).
[17] E. D. Palik and J. K. Furdyna, Rep. Prog. Phys. **33**, 1193 (1970).
[18] A. J. L. Poulter, J. Zeman, D. K. Maude, M. Potemski, G. Martinez, A. Riedel, R. Hey, and K. J. Friedland, Phys. Rev. Lett. **86**, 336 (2001), and references therein.
[19] B. Zhang, M. F. Manger, and E. Batke, Phys. Rev. Lett. **89**, 039703 (2002).
[20] A. J. L. Poulter, C. Faugeras, J. Zeman, M. Potemski, D. K. Maude, and G. Martinez, Phys. Rev. Lett. **89**, 039704 (2002).
[21] S. N. Klimin and J. T. Devreese, Phys. Rev. B **68**, 245303 (2003).
[22] C. K. Patel and R. E. Slusher, Phys. Rev. Lett. **21**, 1563 (1968).
[23] N. Tzoar and E. Foo, Phys. Rev. **180**, 535 (1969).
[24] L. v. Kulik, I. V. Kukushkin, V. E. Kirpichev, K. v. Klitzing, and K. Eberl, Phys. Rev. B **61**, 12717 (2000), and references therein.
[25] V. E. Kirpichev, L. v. Kulik, I. V. Kukushkin, K. v. Klitzing, K. Eberl, and W. Wegscheider, Phys. Rev. B **59**, R12751 (1999).
[26] L. Wendler and R. Pechstedt, J. Phys.: Condens. Matter **2**, 8881 (1990).
[27] J. S. Blakemore, J. Appl. Phys. **53**, R123 (1982).
[28] This is in contrast to the case od 2D systems in which Bernstein modes are more frequently observed (Refs. 24 and 25).
[29] The appearance of the signal due bulk LO phonon could be, however, understood if lowering the temperature and/or increasing the magnetic field splits the sample into two distinct regions, one being insulating and other metallic. (Ref. 30).
[30] F. J. Teran, Y. Chen, M. Potemski, T. Wojtowicz, and G. Karczewski, Phys. Rev. B **73**, 115336 (2006).
[31] C. Faugeras, G. Martinez, A. Riedel, R. Hey, K. J. Friedland, and Yu. Bychkov, Phys. Rev. Lett. **92**, 107403 (2004).
[32] C. Faugeras, G. Martinez, and Yu. Bychkov, Phys. Rev. Lett. **94**, 239702 (2005).
[33] S. N. Klimin and J. T. Devreese, Phys. Rev. Lett. **94**, 239701 (2005).